15TH IEA HEAT PUMP CONFERENCE
MAY 26–29, 2026 | HOFBURG VIENNA 2026
DECARBONISATION THROUGH INNOVATION

System-Level Adsorber Dynamics in Adsorption Heat Pumps: Equilibrium vs. Diffusion Mass-Transfer

Amir Zivariravan[a,b,c,*], Alessia Arteconi[a,c], Giulio Santori[b]

[a]Department of Mechanical Engineering, KU Leuven, Leuven 3000, Belgium
[b]School of Engineering, The University of Edinburgh, Edinburgh EH9 3FB, United Kingdom
[c]EnergyVille, 3600, Genk, Belgium

Abstract

Adsorption heat pumps (AHPs) convert low-grade thermal energy into cooling or heating, but their performance depends on coupled heat and mass transfer in the adsorber. Predictive yet hardware-agnostic models are needed to guide design and operation across different geometries and operating schedules. Here, we apply a dimensionless adsorber framework previously developed by the authors that captures both inter-component and intra-particle transport effects while remaining suitable for cycle-level performance metrics. Intra-particle transport in the adsorber module is treated analytically and embedded in the system balances via a causal convolution kernel. Using the silica gel–water working pair, we (i) compare equilibrium and diffusion-based mass-transfer closures, (ii) map dimensionless time against the governing dimensionless groups, and (iii) propagate the resulting dynamics to cycle-level metrics (specific heating/cooling power and coefficient of performance, COP) through the effective uptake swing, Δq_{eff}, and the cycle time, T_{cyc}. Results show that equilibrium models overpredict specific power when the mass-transfer Biot number and adsorption Damköhler number are small; in contrast, the convolution-kernel closure captures film-limited early-time behavior and diffusive late-time tails. The cycle-level model also indicates that, in the ideal loss-free limit, COP is only weakly sensitive to kinetics, whereas practical COP reductions correlate with the heat-release number and the heat-capacity ratio.

Selection and/or peer-review under the responsibility of the organizers of the 15th IEA Heat Pump Conference 2026.

Keywords: Adsorption heat pump; Heat and mass transfer; Intraparticle diffusion; Dimensionless modelling; Silica gel–water.

1. Introduction and motivation

Adsorption heat pumps (AHPs) upgrade low-grade thermal energy (e.g., waste heat or solar heat) into useful cooling and heating by cycling solid–vapor working pairs. This makes them attractive for flexible refrigerant selection and demand-side decarbonization in thermal systems[1,2]. Their performance is governed by tightly coupled, multiscale transport: vapor exchange among components, heat transfer between the heat-transfer fluid and the adsorbent bed, and mass transport within porous particles[3,4]. These coupled processes shape the transient response during adsorption and desorption, and ultimately determine the system-level figures of merit relevant to design and operation—specific cooling/heating power (SCP/SHP) and coefficient of performance (COP) [5,6].

Modelling approaches for AHP adsorbers typically span two extremes. At one end, equilibrium (or quasi-equilibrium) models assume instantaneous solid–vapor equilibration. These models are computationally efficient and convenient for preliminary sizing and parametric screening, but they inherently suppress finite-rate effects such as film-limited early response and diffusion-induced tails. As a result, they can substantially overpredict SCP/SHP and misestimate cycle times, particularly when external mass-transfer resistance is non-negligible or intraparticle diffusion is slow compared with the bed's convective time scale [7,8]. At the other end, diffusion-aware models explicitly resolve film and intraparticle resistances and can reproduce rate limitations more accurately; however, they often depend on design-specific and operating-condition-specific

* Corresponding author. *E-mail address:* amir.zivariravan@kuleuven.be

details (geometry, coating thickness, porosity, thermal contacts, valve timing, and heat-transfer flow schedules) [9,10]. This dependence introduces many case-specific parameters and boundary conditions, reducing portability across designs and complicating cross-comparison, optimization, and control-oriented use [4,5,11]. In practice, adapting such high-fidelity models to a new configuration frequently requires re-identifying mass-transfer and thermal/vapor resistance parameters, re-meshing, re-tuning numeric, and often additional experiments—substantially increasing modelling time and cost [12,13].

These considerations motivate two practical needs: (i) a portable system model that retains the essential kinetics (film and intraparticle diffusion) without being locked to a particular hardware realization, and (ii) a mathematically consistent mapping from transient adsorber dynamics to cycle-level performance which means a transparent route from the loading history to the realized finite-time uptake swing, Δq_{eff}, the cycle time T_{cyc}, and consequently SCP, SHP, and COP.

To address these needs, this paper makes three contributions:

- Design-agnostic, dimensionless adsorber model with diffusion physics: We develop a portable formulation that embeds an operator-based intraparticle diffusion closure, enabling the model to capture film-influenced early dynamics and diffusion tails while remaining transferable across designs and operating conditions.
- Formal projection from transients to cycle metrics: We provide a consistent projection from transient uptake dynamics to Δq_{eff} and T_{cyc}, and from these to cycle-level performance metrics (SCP/SHP/COP), supplying a justified link that equilibrium-only approaches cannot establish.
- Equilibrium-admissibility and power-bias maps: We introduce power-bias maps β on the Biot–Damköhler plane across multiple dimensionless cycle times Θ_{cyc}(with other dimensionless groups held fixed per comparison). These maps delineate regions where equilibrium closures are admissible and provide actionable design–operation guidance.

Using a representative silica gel–water AHP, we first compare equilibrium and diffusion closures at the system level to identify when equilibrium predictions remain acceptable and when they fail. We then construct utilization maps based on $\eta_u = \Delta q_{\mathrm{eff}}/\Delta q_{\mathrm{eq}}$ to quantify kinetic shortfall as a function of stroke time, and propagate Δq_{eff} and T_{cyc} to generate power maps (SCP/SHP). This framework therefore makes explicit how transient transport limitations translate into cycle performance, while also quantifying equilibrium-induced power overestimation where applicable.

The remainder of the paper is organized as follows. Section 2 presents the governing balances, the kernel/operator-based intraparticle closure, and the dimensionless groups. Section 3 derives the mapping from transient uptake to Δq_{eff}, T_{cyc}, and cycle-level metrics (SCP, SHP, COP). Section 4 describes the numerical method and study design. Section 5 reports results including equilibrium versus diffusion comparisons, power-bias maps, and trends with design and operation insights. Section 6 concludes with practical guidance and key findings.

2. Dimensionless adsorber model and closures

The formulation of a heat and mass transfers for a single adsorber module is expressed in a small set of compact, dimensionless groups that cleanly separate design (hardware and morphology) from operation (flow, temperatures, scheduling). This separation makes the method portable across hardware while enabling fair, like-for-like comparisons. Given an operating schedule of the heat pump cycle (inlet temperature/flow, valve timing), the model provides the transient response and the corresponding adsorbent material surface-equilibrium history; from these we obtain the finite-time uptake swing. We then project transients to cycle level by introducing a nondimensional cycle time. Cycle metrics (SCP, SHP, COP) follow directly from the uptake swing and cycle time, allowing us to assess design vs operation choices and to compare equilibrium and diffusion closures via bias maps over the Biot–Damköhler plane at several dimensionless cycle times.

2.1. Adsorber module model and assumptions

A single adsorber module comprising a convective fluid channel, a wet-adsorber domain (heat exchanger body + adsorbent + adsorbate under local thermal equilibrium), and a vapor plenum is modelled and introduced in [14,15], as illustrated in Figure 1. Flow is 1-D axial in the fluid; axial solid conduction and radiation are neglected. Inter-component vapor paths (valves and lines) are represented by a lumped conductance. The surface uptake $q_{\mathrm{eq}}(t)$ follows the chosen equilibrium isotherm evaluated at the particle surface state.

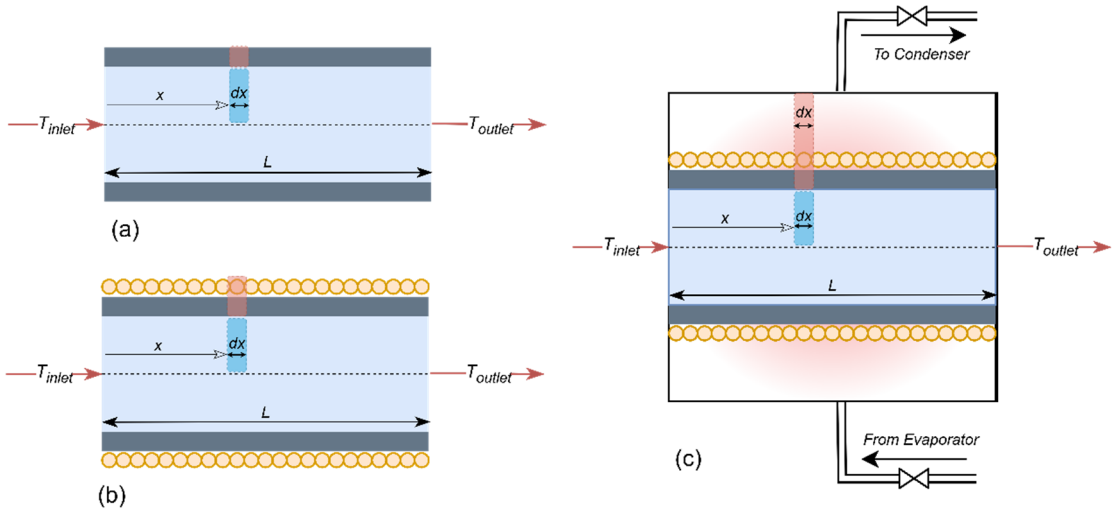

Figure 1. Adsorber module schematic used in this study. (a) Heat-exchanger channel differential element: bulk fluid exchanges heat with the solid matrix through an overall thermal conductance; axial convection is dominant. (b) Dry-adsorber differential element: heat-exchanger wall plus porous solid (no adsorbate), used to define effective thermal capacities and overall conductance. (c) Wet-adsorber domain: heat-exchanger body, porous adsorbent, and adsorbate connected to the vapor circuit via a lumped conductance; film transfer at the particle surface and intraparticle diffusion are shown qualitatively.

2.2. Heat/mass-transfer closures and diffusion-kernel operator

In the coating/packed beds intraparticle transport is Fickian with a finite-film boundary. Eq. (1) is the bed-average uptake as a causal convolution:

$$q(t) = \int_0^t h(t-\tau;\, \mathrm{Bi}_m)\, q_{eq}(\tau)\, d\tau \tag{1}$$

Eq. (1) retains film-affected early response and diffusion-controlled tails with a short eigenmode series in the kernel h [16,17]. The mass-transfer Biot number, $\mathrm{Bi_m} = k_f \ell / D_e$, compares the external (film) mass-transfer resistance to the internal (intraparticle) diffusion resistance [18].

Fluid–solid heat exchange is captured by overall UA, reported via number of transfer unit (NTU). Vapor plumbing is summarized by a vapor conductance number Λ_v(net line/valve conductance scaled by vapor capacitance). Time-proportional and sensible loads are aggregated in a heat-release number Π_H (step-released heat vs available thermal buffer).

2.3. Non-dimensional groups and governing equations

With axial length L, convective time $\tau_c = L/u$, and diffusive time $\tau_d = \ell^2/D_e$, we define $\mathrm{Da}_a = \tau_c/\tau_d$, $\mathrm{Bi}_m = k_f \ell / D_e$, $\mathrm{NTU} = UA/\dot{m}\, c_p$. Design-fixed quantities $(\ell, D_e, UA, \Lambda_v)$ are separated from operation-tunable ones. Let $(\cdot)^*$ denote dimensionless variables and γ_q, Φ_H, χ_v the usual capacity/heat-coupling factors arising from the scaling by the fluid thermal throughput and the module capacities as in Eq. (2):

$$\gamma_q = \frac{\dot{m}\, c_p\, \tau_c}{C_w}, \qquad \Phi_H = \frac{\Delta H_{iso}\, m_{ads}\, q_{ref}}{C_{s,eff}\, \Delta T_{ref}}, \qquad \chi_v \approx \frac{R\, T_{ref}\, m_{ads}\, q_{ref}}{C_v\, \Delta p_{ref}} \tag{2}$$

where $C_w = (\rho_s c_s)_{\mathrm{eff}} V_s$ is the wet-adsorber thermal capacity, C_v is the vapor capacitance [19], and ΔT_{ref}, Δp_{ref}, q_{ref} are the temperature, pressure, and uptake scales used for non-depersonalization (typically the imposed stroke spans and $q_{\mathrm{ref}} = \Delta q_{eq}$). Thus γ_q measures fluid thermal throughput over a convective time relative to the solid's heat buffer, Φ_H weights adsorption heat release against that buffer, and χ_v measures the vapor–uptake coupling relative to vapor capacitance (ideal-gas form shown). The 1-D balances are as Eqs. (3) – (5):

$$\frac{\partial T_f^*}{\partial t^*} + \frac{\partial T_f^*}{\partial x^*} = NTU\,(T_w^* - T_f^*) \tag{3}$$

$$\frac{\partial T_w^*}{\partial t^*} = \gamma_q\, NTU\,(T_f^* - T_w^*) - \Phi_H\, \frac{\partial q^*}{\partial t^*} \tag{4}$$

$$\frac{\partial p^*}{\partial t^*} = \Lambda_v(p_s^*(t^*) - p^*) - \chi_v\, \frac{\partial q^*}{\partial t^*} \tag{5}$$

The system of governing equations is closed by the dimensionless uptake operator in Eq.(6):

$$q^*(t^*) = \int_0^{t^*} h^*(t^* - \tau; \mathrm{Bi}_m, Da_a)\, q_{eq}^*(\tau)\, d\tau \tag{6}$$

Eqs. (3)–(6) are design and operation agnostic where geometry and morphology enter only via $\mathrm{Bi}_m, \mathrm{Da}_a, \mathrm{NTU}, \Lambda_v, \gamma_q$. Typical initial condition for the above-mentioned system of equations are $T_f^*(x,0) = T_{f,0}^*$, $T_w^*(x,0) = T_{w,0}^*$, $p^*(x,0) = p_0^*$, $q^*(0) = q_0^*$. Adsorption/desorption steps are imposed to the solver by time-dependent inlet temperature/flow and vapor conductance; the surface isotherm provides $q_{\mathrm{eq}}^*(t^*)$ from $(p^*(t^*), T_w^*(t^*))$.

3. From transient dynamics to cycle metrics

The goal of this section is to translate the transient adsorber dynamics (Section 2) into the cycle-level figures of merit used for design and operation: specific cooling/heating power (SCP/SHP) and coefficient of performance (COP). A time-varying operating schedule (i.e., the inlet temperature and flow together with the valve conductance) sets the particle-surface pressure/temperature and therefore the surface-equilibrium loading $q_{\mathrm{eq}}(t)$. The bed-average loading $q(t)$ is then obtained by convolving this surface-equilibrium history with the diffusion kernel h using Eq. (1) or (6). Considering symmetric adsorption/desorption steps of duration T_{st} separated by a small but negligible dead time $\varepsilon_{\mathrm{dead}}$ (switching, valve lag), the cycle time is $T_{cyc} = 2\,T_{st}$. Given $q(t)$, the finite-time uptake swing is defined as Eq. (7):

$$\Delta q_{eff} = q_{ads}(T_{st}) - q_{des}(T_{st}), \qquad \eta_u = \frac{\Delta q_{eff}}{\Delta q_{eq}} \in (0,1] \tag{7}$$

where η_u is the utilization factor, i.e., the fraction of the equilibrium swing Δq_{eq} realized within the chosen stroke time T_{st}; in the limit of strong transport (large Bi_m, large Da_a) or sufficiently long strokes, $\eta_u \to 1$. Letting h_{fg}^e and h_{fg}^c denote the latent heats at the evaporator and condenser, and $\bar{h}_{iso}^{ads}$, $\bar{h}_{iso}^{des}$ the averaged isosteric heats of adsorption and desorption and aggregating sensible terms into Q_{sens} the cycle heats per unit adsorbent mass are as in Eqs. (8) and (9) [4]:

$$\frac{Q_e}{m_{ads}} = \Delta q_{eff}\, h_{fg}^e, \qquad \frac{Q_c}{m_{ads}} = \Delta q_{eff}\, h_{fg}^c \tag{8}$$

$$\frac{Q_a}{m_{ads}} \approx \Delta q_{eff}\, \bar{h}_{iso}^{ads}, \qquad \frac{Q_{in}}{m_{ads}} \approx \Delta q_{eff}\, \bar{h}_{iso}^{des} + \frac{Q_{sens}}{m_{ads}} \tag{9}$$

The specific powers (per unit adsorbent mass) then read as Eq. (10), and the COPs can be presented as Eq. (11):

$$SCP = \frac{Q_e}{m_{ads}\, T_{cyc}} = \frac{\Delta q_{eff}\, h_{fg}^e}{T_{cyc}}, \qquad SHP = \frac{Q_a + Q_c}{m_{ads}\, T_{cyc}} = \frac{\Delta q_{eff}(\bar{h}_{iso}^{ads} + h_{fg}^c)}{T_{cyc}} \tag{10}$$

$$COP_{cool} = \frac{Q_e}{Q_{in}} \approx \frac{h_{fg}^{e}}{\bar{h}_{iso}^{des} + Q_{sens}/(\Delta q_{eff} m_{ads})}, COP_{heat} \approx \frac{\bar{h}_{iso}^{ads} + h_{fg}^{c}}{\bar{h}_{iso}^{des} + Q_{sens}/(\Delta q_{eff} m_{ads})} \quad (11)$$

A useful normalization for cross-design comparison is in Eq. (12) which depends only on the dimensionless groups $\{\mathrm{Bi}_m, \mathrm{Da}_a, \mathrm{NTU}_q, \Lambda_v, \gamma_q\}$

$$SCP^{*} = \frac{SCP\,\tau_c}{h_{fg}^{e}}, \qquad SHP^{*} = \frac{SHP\,\tau_c}{\bar{h}_{iso}^{ads} + h_{fg}^{c}} \quad (12)$$

Two consequences follow immediately. (i) Ideal loss-free limit: If sensible terms are negligible ($Q_{\mathrm{sens}} \to 0$), the Δq_{eff} factor cancels in (11), so COPs are weakly sensitive to kinetics, whereas SCP/SHP scale with both Δq_{eff} and the cycle frequency $1/T_{\mathrm{cyc}}$. (ii) Equilibrium bias: If one computes Δq_{eff} with an equilibrium closure in place of the diffusion operator, the specific powers are over-estimated at fixed T_{st}. A convenient bias metric is defined in Eq. (13) to measure the deviation of non-equilibrium specific powers from the equilibrium ones.

$$\beta = \frac{SCP^{\,eq}}{SCP^{\,diff}} = \frac{\Delta q_{eff}^{eq}}{\Delta q_{eff}^{diff}} = \frac{1}{\eta_u} \geq 1 \quad (13)$$

Finally, choosing the half cycle time T_{st} is a trade-off between utilization and frequency. For a given boundary span, an operationally transparent rule can be as (14):

$$T_{st}^{\star} = \min \left\{ T_{st} : \eta_u(T_{st}) \geqslant \eta_{\min} \right\} \quad (14)$$

with $\eta_{\min} \approx 0.85$–0.9 when an equilibrium closure is desired; otherwise the diffusion operator should be retained. In Section 5 we visualize these trade-offs as regime maps over $(\mathrm{Bi_m}, \mathrm{Da_a})$, showing how increases in film coefficient k_f and effective diffusivity D_e move a design toward higher utilization, higher power, and—when Π_H is small—near-ideal COP.

4. Numerical solution and study setup

4.1. Spatial discretization and time integration

The one-dimensional balances (3)-(6) are solved on a uniform axial grid using a conservative finite-difference form for the fluid energy and a collocated point for the wet-adsorber energy and vapor mass. Time integration is semi-implicit (backward differencing for the source/exchange terms; first-order upwind for the convective term in T_f); nonlinearities are treated with Newton iterations and a line search [20]. At each step, the uptake operator is evaluated by recursive kernel updates (no history storage beyond the modal states). Convergence criteria are $\| R \|_2 / \| R_0 \|_2 \leq 10^{-8}, \max | \Delta \mathbf{y} | \leq 10^{-9}$ with $\mathbf{y} = [T_f, T_w, p, q]^{\mathsf{T}}$. The time step Δt is adapted to keep $\max | \Delta q | / | q | \leq 1\%$ and to confirm a CFL-like condition for the fluid convection.

The diffusion kernel $h(\cdot; \mathrm{Bi_m})$ is represented by the standard slab-with-film eigenmodes [21,22]; we retain the smallest M eigenvalues such that the modal tail at the end of a cycle is negligible in Eq. (15)

$$\exp(-\lambda_M^2\, t_{\mathrm{end}}/\tau_d) \leq \varepsilon_{\mathrm{ker}}, \varepsilon_{\mathrm{ker}} = 10^{-6} \quad (15)$$

where λ_M is the M-th Robin eigenvalue and $\tau_d = \ell^2/D_e$ [21].This control ensures that early film-affected behavior and late diffusive tails are captured without term-by-term series evaluation.

4.2. Numerical convergence assessment

A structured mesh and time-step refinement study was performed to quantify numerical error in the key outputs used throughout (step time t_{90}^{*}, utilization η_u, and cycle metrics). The axial grid was refined

uniformly by factors of 2 and 4 relative to the baseline ($N_x, 2N_x, 4N_x$); the time step was reduced proportionally to keep the convective CFL number $\mathrm{CFL} = u\,\Delta t/\Delta x \leq 0.5$.

Across representative cases spanning the $(\mathrm{Bi}_m, \mathrm{Da}_a)$ range, refining from N_x to $4N_x$ changed t_{90}^* by $< 0.2\%$, η_u by $< 0.3\%$, and SCP^* by $< 0.5\%$. The adaptive controller limits the per-step relative change in uptake to $\leq 1\%$ (i.e., $\max\ |\Delta q\ |/|\ q\ | \leq 1\%$), which yields nondimensional timesteps $\Delta t/\tau_c \approx 1 \times 10^{-3}$–$5 \times 10^{-3}$. Halving Δt at fixed grid changed t_{90}^* by < 0.1%, η_u by < 0.2%, and SCP^* by < 0.3%. This confirms first-order time accuracy and that the reported trends are insensitive to timestep choice.

Tightening Eq. (14) from $\varepsilon_{\mathrm{ker}} = 10^{-6}$ to 10^{-8} (or increasing M by +5 modes) altered $q(t)$ by $< 10^{-4}$, Δq_{eff} by $< 0.01\%$, and downstream metrics by $< 0.05\%$; thus $M = 8 - 12$ is sufficient over the explored Bi_m. Collectively, these tests bound the numerical uncertainty well below the variations discussed in Section 5, supporting the robustness of the reported β-maps and cycle-level metrics.

4.3. Working pair, operating schedule, and cycle-time definition

The working pair is silica gel–water. The equilibrium relation at the particle surface is provided by a Dubinin–Astakhov-type isotherm evaluated at $(p(t), T_w(t))$[23]. The latent heats h_{fg}^e, h_{fg}^c and the stroke-averaged isosteric heats $\bar{h}_{\mathrm{iso}}^{ads}, \bar{h}_{\mathrm{iso}}^{des}$enter the cycle metrics by the formulations introduced in the section 3 and are treated as known functions of operating conditions. The cycle duration is normalized by the same convective time $\tau_c = L/u$ to define $\Theta_{\mathrm{cyc}} \coloneqq T_{\mathrm{cyc}}/\tau_c$. A finite set of representative Θ_{cyc} levels is selected. For each level, stroke durations and ramps are scaled consistently with the recorded schedule shape.

5. Results: equilibrium admissibility and power-bias maps

Figure 2 summarizes how the power-bias $\beta = \mathrm{SCP}^{eq}/\mathrm{SCP}^{diff}$ (Eq. 13) varies over Biot–Damköhler plane at several dimensionless cycle times $\Theta_{cyc} = T_{cyc}/\tau_c$. Each panel fixes one Θ_{cyc}; the horizontal axis is Bi_m and the vertical axis is Da_a, both on log scales. Symbols mark evaluated operating points and the colour field is an interpolation drawn only inside the convex hull of the data. White diagonal lines are $\mathrm{Bi}_m.\mathrm{Da}_a$ isolines. Other dimensionless groups remain at their case values while we compare $(\mathrm{Bi}_m, \mathrm{Da}_a)$ across Θ_{cyc}. By definition $\beta \geq 1$; values near 1 indicate that the equilibrium closure and the diffusion operator predict similar specific cooling power under the same schedule, whereas high β marks conditions where the equilibrium closure over-predicts power. The global pattern is consistent across panels: large β at small Bi_m and small Da_a; $\beta \to 1$ as both numbers increase.

The trends follow directly from transport physics. Increasing Bi_m weakens the external film resistance, which reduces the early-time uptake lag that the diffusion operator captures and the equilibrium closure misses; β therefore decreases along the Bi_maxis. Increasing Da_a shortens the intraparticle diffusion time relative to the convective time, which damps the long diffusive tail and again reduces β. Because film and intraparticle resistances act in series, the steepest reduction of β occurs along a diagonal move toward higher Bi_m and higher Da_a [22,24,25]. Cycle time sets how far dynamics can relax within one cycle. Short cycles (small Θ_{cyc}) leave less time for uptake to approach the equilibrium swing, so Δq_{eff}^{diff} is smaller and β is larger. As Θ_{cyc} increases, η_u increases, the diffusion result approaches the equilibrium swing, and β approaches 1 over a wider area. These observations are consistent with Eqs. (8) and (10): power scales with $\Delta q_{eff}/T_{cyc}$, and the diffusion closure mainly changes Δq_{eff} at fixed schedule.

For practice, a simple acceptance frontier such as $\beta \leq 1.05$ or $\beta \leq 1.10$ can be used to decide when an equilibrium closure is adequate at a given Θ_{cyc}. This aligns with the utilisation rule in Eq. (14), since near $\eta_u = 1$ the bias and the utilization shortfall are directly related. The maps also suggest how to move across the frontier. Rightward motion arises from higher k_f through channel design or surface treatment; upward-right motion comes from higher D_e or smaller ℓ. Higher flow increases Da_a and often improves NTU, but film scaling must be checked so that Bi_m does not fall. Improving NTU limits γ_q so kinetics, not thermal drift, sets the achievable power. The bias concerns SCP and SHP at fixed schedule; ideal COP remains weakly sensitive to kinetics as discussed in Section 3. We restrict interpretation to the region covered by data points, and do not extrapolate beyond the convex hull.

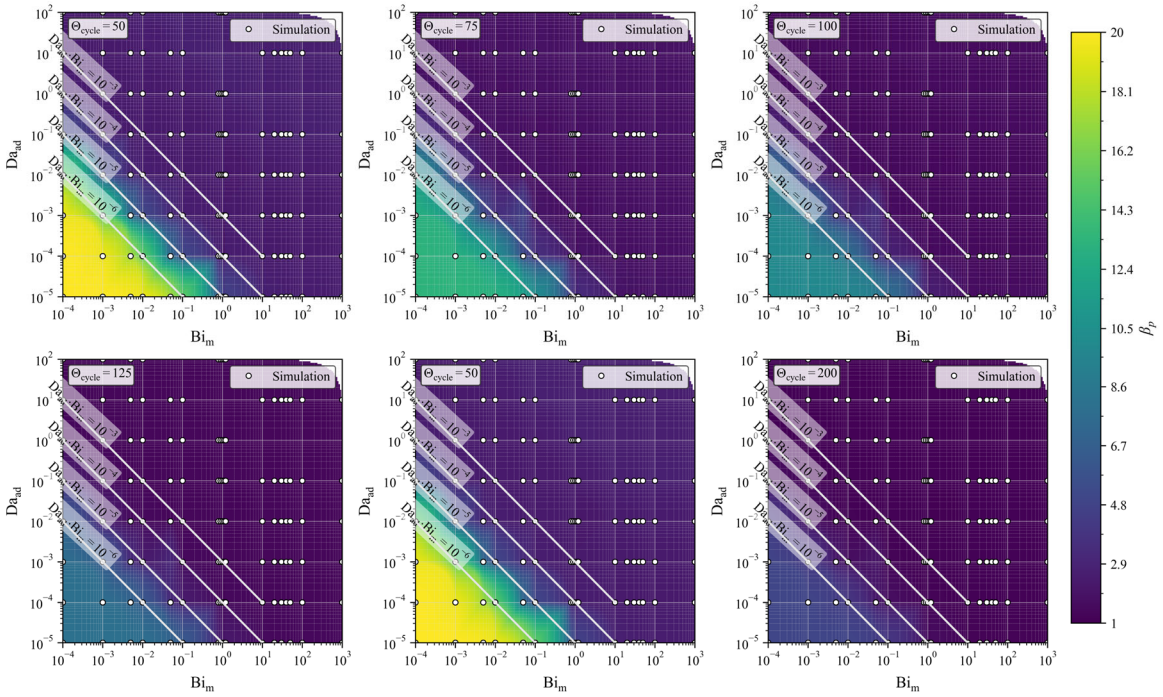

Figure 2. Power-bias $\beta(\mathrm{Bi_m}, \mathrm{Da_a}; \Theta_{\mathrm{cyc}})$ at six dimensionless cycle times. Colour shows $\beta = SCP^{eq}/SCP^{diff}$. Panels correspond to $\Theta_{cyc} = 50, 75, 100, 125, 150, 200$. Axes: $\mathrm{Bi_m}$(horizontal, log) and $\mathrm{Da_a}$(vertical, log). Symbols are data points; shading is interpolation. $\mathrm{Bi_m}$. $\mathrm{Da_a}$ isolines are shown for reference and also for suggesting how to move across the frontier.

6. Conclusions and practical design guidance

We present a design and operation agnostic, dimensionless adsorber framework that embeds an operator-based intraparticle diffusion closure and projects transient behavior to cycle performance (SCP, SHP, COP) through the effective swing Δq_{eff} and cycle time T_{cyc}. Using this framework, we assemble power-bias maps $\beta = \mathrm{SCP^{eq}}/\mathrm{SCP^{diff}}$ over $(\mathrm{Bi}_m, \mathrm{Da}_a)$ at several dimensionless cycle times Θ_{cyc}, with other dimensionless groups held fixed to enable fair comparison. The maps delineate where an equilibrium closure is admissible and provide concise guidance for design and operation. In practice, selecting the stroke time by a utilization rule (e.g., $\eta_u \geq 0.9$)—equivalently $\beta \leq 1.05$–1.10 at the intended Θ_{cyc}—offers a simple acceptance criterion; moving toward higher Bi_m and Da_a (via improved film transfer, higher effective diffusivity, or shorter diffusion length) expands this admissible region. Together, the β-maps and the η_u criterion form a portable basis for benchmarking designs and co-optimizing hardware and operation in adsorption heat-pump systems.

Acknowledgements

The authors would like to thank Bijzonder Onderzoeksfonds (GPUE/21/028) of KU Leuven and the Global PhD Scholarship of The University of Edinburgh for supporting the studentship of Amir Zivariravan; and the Royal Academy of Engineering for the Industry Fellowship in Data Centre Cooling of Giulio Santori (IF2223B-126).

Further, during the preparation of this work the authors used ELM–the University of Edinburgh's AI innovation platform–in order to improve the English language proficiency of the manuscript. After using this tool, the authors reviewed and edited the content as needed and take full responsibility for the content of the published article.

Symbol	Description
Bi_m	Mass-transfer Biot number (film vs intraparticle resistance), dimensionless
c_p	Specific heat at constant pressure of heat-transfer fluid, J kg^{-1} K^{-1}
C_v	Vapor capacitance, kg Pa^{-1}
C_w	Wet-adsorber thermal capacity, J K^{-1}
Da_a	Adsorption Damkohler number, dimensionless
D_{eff}	Effective intraparticle mass diffusivity, m^2 s^{-1}
h_{fg}	Latent heat (evaporator or condenser), J kg^{-1}
h_{iso}	Isosteric heat of adsorption/desorption (stroke-averaged where used), J kg^{-1}
K(t)	Intraparticle diffusion kernel (convolution kernel)
k_f	Film mass-transfer coefficient, m s^{-1}
L	Heat exchanger flow-path length, m
ℓ	Characteristic half-thickness of adsorbent slab/particle, m
NTU	Number of transfer units in the adsorber, dimensionless
p	Pressure, Pa
q(t)	Bed-average solid loading, kg kg^{-1}
$q_{eq}(t)$	Surface-equilibrium loading, kg kg^{-1}
SCP, SHP	Specific cooling/heating power per adsorbent mass, W kg^{-1}
t	Time, s
t_{cyc}	Cycle time, s
t_{st}	Stroke (step) time, s
UA	Overall heat transfer conductance, W K^{-1}
u	Velocity, m s^{-1}
x	Axial coordinate, m
Greek symbols	
β_p	Power bias (equilibrium vs diffusion prediction), dimensionless
γ_q	Vapor-uptake coupling factor (as defined in the scaling), dimensionless
Δq_{eff}	Effective (finite-time) uptake swing, kg kg^{-1}
Δq_{eq}	Equilibrium uptake swing, kg kg^{-1}
ε_{dead}	Dimensionless dead time (switching/valve lag), if used
ε_{ker}	Kernel truncation tolerance, if used
η_u	Utilization factor (fraction of equilibrium swing realized), dimensionless
Θ	Dimensionless time, t/τ_c, dimensionless (if used explicitly)
Θ_{cyc}	Dimensionless cycle time, t_{cyc}/τ_c, dimensionless
Λ_v	Vapor-path conductance number, dimensionless
λ_n	Robin eigenvalue (kernel eigenmode), dimensionale
ρ	Density, kg m^{-3}
τ_c	Characteristic convective time, s
τ_d	Characteristic diffusion time, s
Φ_H	Heat-release number, dimensionless
χ_v	Vapor-pressure coupling number, dimensionless
Subscripts	
0	Initial state
a	Adsorption (for dimensionless groups where used)
ads	Adsorption
c	Condenser
cyc	Cycle
des	Desorption
e	Evaporator
eff	Effective
eq	Equilibrium
f	Heat-transfer fluid, film
fg	Latent heat of vaporization
iso	Isosteric
ker	Kernel
st	Stroke (step)
v	Vapor
w	Wet adsorber / wet domain

References

[1] F. Meunier, Adsorption heat powered heat pumps, Appl. Therm. Eng. 61 (2013) 830–836. https://doi.org/10.1016/j.applthermaleng.2013.04.050.

[2] J.M. Pinheiro, S. Salústio, J. Rocha, A.A. Valente, C.M. Silva, Adsorption heat pumps for heating applications, Renewable and Sustainable Energy Reviews 119 (2020) 109528. https://doi.org/10.1016/j.rser.2019.109528.

[3] J.M.S. Dias, V.A.F. Costa, Adsorption heat pumps for heating applications: A review of current state, literature gaps and development challenges, Renewable and Sustainable Energy Reviews 98 (2018) 317–327. https://doi.org/10.1016/j.rser.2018.09.026.

[4] D.B. Boman, A.W. Raymond, S. Garimella, Adsorption Heat Pumps, Springer International Publishing, Cham, 2021. https://doi.org/10.1007/978-3-030-72180-0.

[5] A. Pesaran, H. Lee, Y. Hwang, R. Radermacher, H.H. Chun, Review article: Numerical simulation of adsorption heat pumps, Energy 100 (2016) 310–320. https://doi.org/10.1016/j.energy.2016.01.103.

[6] S.H. Seol, K. Nagano, J. Togawa, Modeling of adsorption heat pump system based on experimental estimation of heat and mass transfer coefficients, Appl. Therm. Eng. 171 (2020). https://doi.org/10.1016/j.applthermaleng.2020.115089.

[7] V. Palomba, S. Nowak, B. Dawoud, A. Frazzica, Dynamic modelling of Adsorption systems: a comprehensive calibrateddataset for heat pump and storage applications, J. Energy Storage 33 (2021). https://doi.org/10.1016/j.est.2020.102148.

[8] G. Cacciola, G. Restuccia, Reversible adsorption heat pump: a thermodynamic model, International Journal of Refrigeration 18 (1995) 100–106. https://doi.org/10.1016/0140-7007(94)00005-I.

[9] L.Z. Zhang, A three-dimensional non-equilibrium model for an intermittent adsorption cooling system, Solar Energy 69 (2000) 27–35. https://doi.org/10.1016/S0038-092X(00)00010-4.

[10] S. Brandani, E. Mangano, The zero length column technique to measure adsorption equilibrium and kinetics: lessons learnt from 30 years of experience, Adsorption 27 (2021) 319–351. https://doi.org/10.1007/s10450-020-00273-w.

[11] M. Dawoud, A. Mugnini, A. Arteconi, Fast Explicit Formulations of Propane Thermophysical Properties for Dynamic Modelling, Energies (Basel). 19 (2026) 892. https://doi.org/10.3390/en19040892.

[12] A.W. Raymond, S. Garimella, Distributed parameter simulation of annular-finned tube sorption bed, Int. J. Heat Mass Transf. 166 (2021) 120755. https://doi.org/10.1016/j.ijheatmasstransfer.2020.120755.

[13] A. Raymond, S. Garimella, Intraparticle Mass Transfer in Adsorption Heat Pumps: Limitations of the Linear Driving Force Approximation, J. Heat Transfer 133 (2011) 042001. https://doi.org/10.1115/1.4001310.

[14] A. Zivariravan, G. Santori, A. Arteconi, Dynamic Analysis of Adsorption Heat Transformation: A Dimensionless Model Approach for Comparative Evaluation of Sorption Bed Designs, in: Proceedings of the 18th UK Heat Transfer Conference, The University of Birmingham (bham.ac.uk), 2024: pp. 11–13.

[15] A. Zivariravan, G. Santori, A. Arteconi, A dimensionless framework for adsorber dynamics, Thermal Science and Engineering Progress (2026) 104569. https://doi.org/10.1016/j.tsep.2026.104569.

[16] P.J. Davis, P. Rabinowitz, Methods of Numerical Integration, 2nd ed., Academic Press, 2014.

[17] W.H. Press, S.A. Teukolsky, W.T. Vetterling, B.P. Flannery, Numerical recipes: the art of scientific computing, 3rd Edition, Cambridge University Press, 2007.

[18] M. Parti, MASS TRANSFER BlOT NUMBERS, Periodica Polytechnica Mechanical Engineering 38 (1994) 109–122. https://doi.org/N/A.

[19] W. Steckelmacher, A review of the molecular flow conductance for systems of tubes and components and the measurement of pumping speed, Vacuum 16 (1966) 561–584. https://doi.org/10.1016/0042-207X(66)91416-3.

[20] J. Crank, P. Nicolson, A practical method for numerical evaluation of solutions of partial differential equations of the heat-conduction type, Mathematical Proceedings of the Cambridge Philosophical Society 43 (1947) 50–67. https://doi.org/10.1017/S0305004100023197.

[21] F. Erdoğdu, Mathematical approaches for use of analytical solutions in experimental determination of heat and mass transfer parameters, J. Food Eng. 68 (2005) 233–238. https://doi.org/10.1016/j.jfoodeng.2004.05.038.

[22] D.T. Gillespie, E. Seitaridou, The Fickian theory of diffusion, in: Simple Brownian Diffusion, 2nd ed., Oxford University Press, 2012: pp. 1–17. https://doi.org/10.1093/acprof:oso/9780199664504.003.0001.

[23] M.M. Dubinin, V.A. Astakhov, Development of the concepts of volume filling of micropores in the adsorption of gases and vapors by microporous adsorbents, Bulletin of the Academy of Sciences of the USSR Division of Chemical Science 20 (1971) 3–7. https://doi.org/10.1007/BF00849307.

[24] S.A. Adegunju, P.B.C.A. Amalraj, C.E. Holland, M.A. Nicholson, A.D. Ebner, J.A. Ritter, Assessment of the new kinetically limited linear driving force model for predicting diffusion limited adsorption breakthrough curves, Adsorption 30 (2024) 57–77. https://doi.org/10.1007/s10450-023-00434-7.

[25] S. Brandani, E. Mangano, Modelling combined diffusion and surface resistances in adsorbent particles: zero length column for spherical and slab geometries, Adsorption 31 (2025). https://doi.org/10.1007/s10450-024-00557-5.